We are IntechOpen,
the world's leading publisher of
Open Access books
Built by scientists, for scientists

4,800
Open access books available

122,000
International authors and editors

135M
Downloads

154
Countries delivered to

Our authors are among the

TOP 1%
most cited scientists

12.2%
Contributors from top 500 universities

BOOK CITATION INDEX INDEXED
CLARIVATE ANALYTICS

WEB OF SCIENCE™

Selection of our books indexed in the Book Citation Index
in Web of Science™ Core Collection (BKCI)

Interested in publishing with us?
Contact book.department@intechopen.com

Numbers displayed above are based on latest data collected.
For more information visit www.intechopen.com

Chapter

Thousand kW High-Temperature Solar Furnace in Parkent (Uzbekistan) – Energetical Characteristics

Akbarov Rasul

Abstract

This chapter presents a method of calculation of the energetical characteristics of the large solar furnace with a capacity of 1000 kW (LSF) taking into account its real optical parameters. The technical characteristics of the LSF are presented. The possible energy characteristics of the LSF based on numerical calculations are analyzed. The energy characteristics of the total system with different inaccuracies of the reflecting surfaces, energy contributions of certain shelves and groups of heliostats, and the contributions of certain heliostats and shapes of their focal spot are determined. Empirical formulas are proposed to describe the obtained numerical results. The problem of implementing the possible energy modes of the LSF with and/or without the inclusion of certain shelves and groups of heliostats is analyzed. The problem of a day changes in the energy density distribution in the focal spot of the LSF is considered.

Keywords: solar radiation, thermal power, furnace, concentrator, heliostat, focal zone, energy distribution, numerical calculation

1. Introduction

One of the promising directions in the use of solar energy is materials science. As is known, high-temperature heating by solar radiation has certain advantages, e.g., the absence of pollution from synthesized materials, instantaneous heating, the possibility to control the heating and cooling rate, a wide range of solar radiation, etc. At present, high-temperature solar technologies are widely applied in many areas of science and engineering. In this respect, concentrated solar energy is an important component among the available material synthesis methods with a set of specified properties [1–8].

The important characteristics of the technological processes are the capacity, maximum and average energy densities, uniformity of the energy density distribution, focal spot size, character of the energy density distribution and its change in time, duration of the process, start and stop mode rate, etc.

A characteristic drawback of solar concentrators is variability of the characteristics of the focal spot with time. This is related, on the one hand, with the temporary change in the direct solar radiation value, and on the other hand, with the condition of the optical and mechanical elements of solar furnaces, i.e., the adjustment

condition of the mirrors, angular inaccuracies of the light-reflecting mirrors, reflection coefficient of the mirrors, condition of the solar sensors, etc.

The Materials Science Institute of the Academy of Sciences of the Republic of Uzbekistan operates a large solar furnace of 1000 kW thermal power (LSF). It is a composite optical and mechanical complex with automatic control systems, comprising the heliostat field (62 heliostats), paraboloidal concentrator (with 1906 m^2 midship section area-projection of the surface of the concentrator on the plane), and technological tower. Highly concentrated solar radiation, with energy density up to 700 W/cm^2, may be nowadays created in the focal region of the LSF, located in the technological tower. A set of specialized testing facilities are developed at the LSF, having not analogues in terms of a number of parameters either in home or foreign practice. Note that the abbreviation BSF (Big Solar Furnace) is often used instead of the LSF.

The LSF was put into operation as an experimental-industrial one, in the summer of 1987 [9, 10].

During Soviet times this unique solar furnace was the leading facility of military-industrial complex for testing of different materials and equipment to the action of concentrated solar radiation and for development of advanced ceramic materials for high-tech industry.

In connection with the change of research direction (from military to peaceful), the fields of technology of engineering ceramics, fireproof materials of wide range of applications, particularly for metallurgy, oil and gas complex, power engineering, machine building, and chemical industries became the major directions of use of LSF.

Scientists in Uzbekistan have achieved significant results in high-temperature solar technologies. More than 150 compositions of various oxide materials having unique properties and serving as the basis for functional, structural, and high-refractory ceramics have been developed and synthesized at the LSF, and their thermophysical and other characteristics have been studied. The LSF is a unique instrument for field studies of high-temperature processes, i.e., on the synthesis and heat treatment of materials and study of their properties.

Note that such a furnace was previously commissioned in Odeillo, France. This 1000 kW solar furnace was completed in 1970 (**Figure 1**). The furnace contains 63 orientated mirrors (heliostats), each of 45 m^2 surface, with 180 single mirror

Figure 1.
General view of the France furnace.

panes (facets). The movement of this installation is guided by electronic controls operated by reflected rays. The accuracy of the control is 1 min of arc, but due to dispersion on the flat glass, 5 min of arc are obtained on the reflected rays. A solar beam of constant energy is directly horizontally southward to a paraboloid reflector of 2000 m² intercepted area. This paraboloid contains 9500 single glass panes, bent by mechanical constraint and adjusted to reflect maximum radiation to the focal plane, situated 18 m from the apex of the parabola [3, 4, 11].

Technological capabilities of the furnace are described in the works [2–5].

2. Main technical characteristics of the LSF

The LSF as noted above represents a complex optomechanical aggregate with automatic control systems consisting of a heliostat field and paraboloid concentrator, which form a high-density radiation flux in the focal zone of the concentrator. The furnace is located 50 km from Tashkent, in the Parkent District. The geographical location is 41.32°N, 69.74°E; its altitude above sea level is 1050 m.

The LSF heliostat field is formed by 62 heliostats located on the smooth slope of a mountain (slope 13°) in a checkerboard pattern arranged on 8 terraces. All 62 heliostats of the LSF have a similar structure and dimension. The reflecting surface of the heliostat with dimensions of 7.5 × 6.5 m is flat and composite and consists of 195 facets with dimensions of 0.5 × 0.5 m and a thickness of 6 mm.
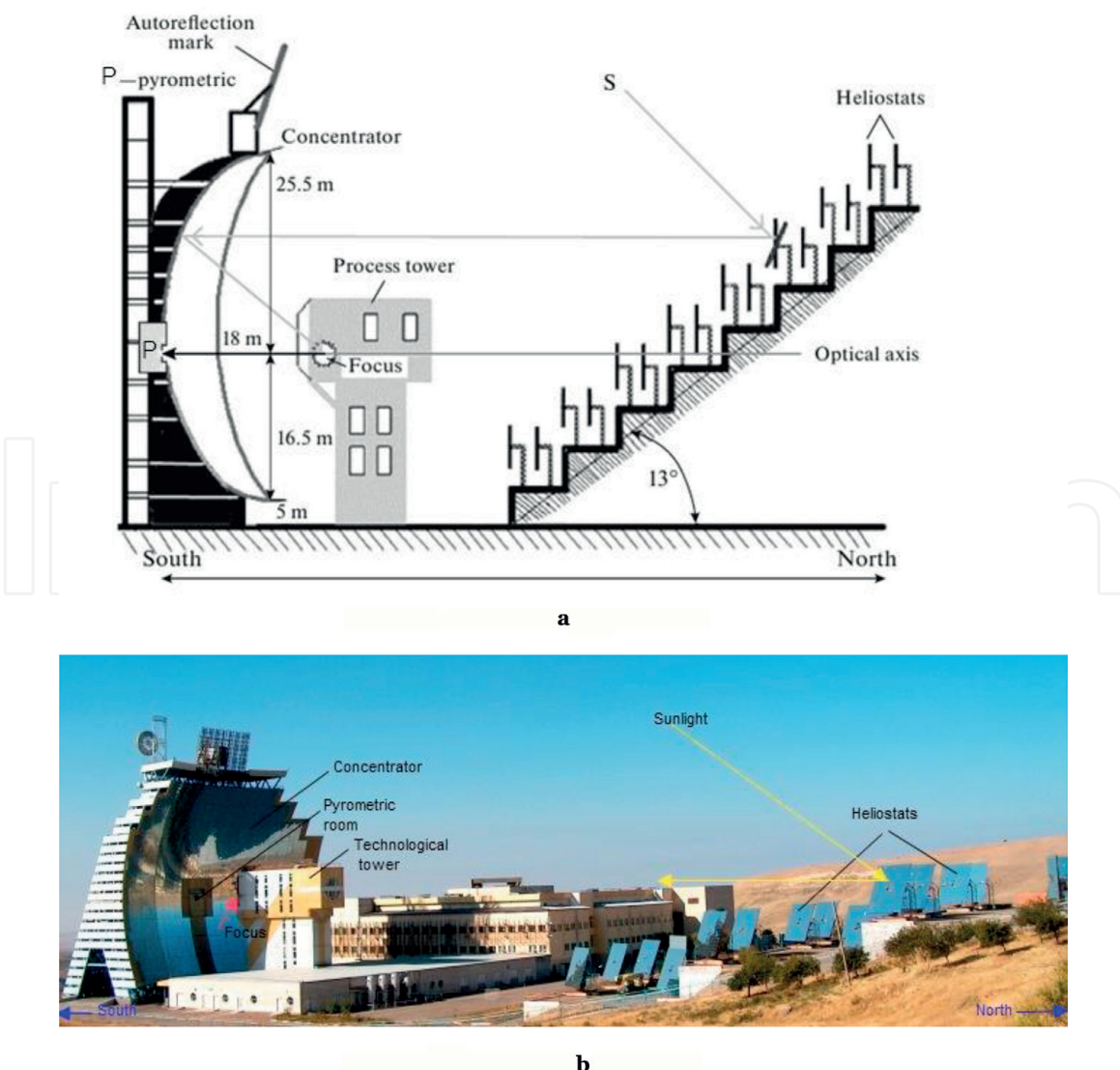

Figure 2.
(a) Overview diagram of LSF and (b) general view of the LSF.

The reflecting surface of the concentrator is a rectangular-stepped cutting of a paraboloid of revolution with a focal distance of 18 m. The height of the midsection of the concentrator is 42 m, and the width is 54 m. The total area of the midsection of the reflecting surface is 1906 m^2. The concentrator consists of 214 blocks. 50 rhomb-shaped facets with sides of 447 mm and different apex angles are installed on each block. The thickness of mirrors is 5 mm.

In total, there are 22,790 facets; the total area of the reflecting mirrors (facets) is about 5200 m^2; the heliostat field, process tower, and concentrator occupy approximately 2 ha of ground area. Technical characteristics of the installation are also described in the works [9, 10, 12, 13].

The general pattern of the device is shown in **Figure 2a** and the general view of the installation were shown in **Figure 2b**.

3. Operating experience of the LSF

Some advantages of the LSF should be noted as compared with other solar furnaces, resulting from the specific nature of the optical circuit of the furnace and latest engineering developments used in the furnace's operation: the heliostat automated control system (HACS), computer vision system (CVS), photometers, radiometers, melting furnaces of different designs, modern meteorological station in the territory of the furnace, high-accuracy methods for arranging the furnace's reflecting mirrors, various tests and optical benches, etc [14–21].

Some projects have been implemented in recent years at the entity "Sun" of the Academy of Sciences of the Republic of Uzbekistan, where the LSF is located; the aim of these projects is to improve its operational characteristics and extend its functional capabilities.

One of the most significant finished projects is the commissioning of the modern meteorological station on the territory of the "Sun" entity in 2013 with the financial support of the Asian Development Bank. This station is equipped with high-frequency pyranometers and pyrheliometers to measure solar radiation. The station measures global horizontal radiation and diffuse horizontal and beam normal solar radiation [20]. As is known, beam normal solar radiation is important for the LSF, and depending on its level, it is possible to implement certain high-temperature processes. With the commissioning of the meteorological station, it is possible to define more correctly and promptly the energy characteristics of the furnace using the calibration coefficients. Certain types of operations, such as, preventive maintenance, adjustment and cleaning of the reflecting elements, regulation of the solar sensors of the heliostats, different high-temperature processes requiring certain process modes in the focal zone of the furnace, etc., are performed at the LSF depending on the climatic conditions and solar radiation level. With the intensive operation of the LSF, planning of the work on it is important, and the selection of the type of operations is primarily related to the radiation environment of the location. For example, according to long-term observations, many high-temperature processes are carried out when the beam solar radiation has a value of 600 W/m^2 or larger. At present, various types of operations are planned in advance at the LSF according to the time of day and season based on statistical processing of meteorological data.

Efficient operation of the LSF significantly depends on the technical parameters of the HACS for tracking the Sun due to the specific nature of its optical circuit. At present, the capabilities of the existing HACS developed from outmoded element bases do not meet modern requirements, although it functions. This is why a new modern HACS has been developed at the LSF in recent years; this will make it

possible to significantly extend its functional capabilities. The new HACS differs fundamentally from the old one: modern microprocessor circuits are used in the element bases, achievements in modern information technologies have been implemented, reliable operation is ensured, and it has high accuracy and flexibility for the required processing modes [19]. The operational efficiency of the new system has successfully been tested on one heliostat, and efforts on transferring the system to other heliostats are planned (2019-2020). As a result, the LSF will have some new possibilities for practical use.

It should be noted that the third modernization of the control system of the heliostats of the French furnace has also been completed recently [22].

Furthermore, any complex processing device without a system for monitoring and measuring its operating parameters and characteristics cannot function efficiently and reliably. In this respect, the LSF is equipped with modern devices to measure the density of concentrated solar energy and the temperature of the studied materials and devices to control the behavior of the high-temperature processes. They include a high-temperature pyrometer for remote measurement of the temperature of materials (IMPAC IGA 12, T_{max} = 3500°C), a thermal imager (FLIR A655), various radiometers, photometers, digital thermometers, a computer vision system (developments of the Institute of Materials Science - IMS) and etc.

Thus, the LSF, in addition to an environmentally friendly melting furnace, is a unique research tool for high-temperature studies, which has some important advantages compared to other high-temperature solar furnaces:

1. High power of the furnace, up to 1 MW.

2. High levels of solar radiation concentration, $\approx$ 4500–10,000.

3. Large size of the focal spot of the furnace, $\approx$ 80–100 cm.

4. Sixty-two heliostats, which makes it possible to control the focal energy distribution.

5. The HACS makes it possible to flexibly control movement of the heliostats.

6. Simulation of 62 aperture-specific concentrators.

7. Control of the behavior of technological processes.

8. The ability to measure and control the optical energy condition of the furnace.

4. Calculation of the optical-energetical characteristics of the LSF: the general approach

In the helio-engineering practice, different techniques for evaluation of energetical characteristics of mirror concentrating systems (MCS) are employed, depending on the purpose, demanded accuracy, etc [23–29]. However, if a big MCS as a solar furnace in Odeillo (France) or Large Solar Furnace near Tashkent (Uzbekistan) is concerned, there are specific features which must be taken into account.

An important feature of a big-scale MCS is the use of multi-heliostat system to create illumination field on its focal zone. Thanks to this feature, there is a

possibility of a flexible control upon flux density distribution by individual control of each heliostat operation regime. This is a very important point for many technological processes and special investigations.

Exposure distribution of the whole system is the sum of individual exposure distributions created by particular heliostats. Because of this fact, it is enough to consider the problem of illumination distribution created by a particular heliostat for arbitrary moment and given direction of beams reflected from the heliostat.

We will use the Cartesian coordinate system with axes: X (direction to Zenith), Y (to West) and Z (to South); the center of this system is in the focus of the furnace. Let the direction of beams reflected from the heliostat be characterized by a unit vector $\vec{K}$ (K_x, K_y, K_z). Then the unit vector of the heliostat's normal is determined by the expression

$$\vec{N_g} = \frac{\vec{S} + \vec{K}}{\sqrt{2\left(1 + \vec{S}\vec{K}\right)}}$$

where $\vec{S}$ is the coordinate of the Sun's unit vector

$$S_x = \sin h_s = \cos\varphi \cos\delta \cos kt + \sin\varphi \sin\delta$$
$$S_y = \cos h_s \sin A_s = \cos\delta \sin kt$$
$$S_z = \cos h_s \cos A_s = \sin\varphi \cos\delta \cos kt - \cos\varphi \sin\delta$$

where δ is the declination of the Sun, k = 15 deg./h, φ is the geographical latitude, and t is time.

The angle coordinates of the heliostat A_n and h_n are determined by expressions

$$N_{gx} = \sin h_n, \quad N_{gy} = \cos h_n \cos A_n, \quad N_{gz} = \cos h_n \sin A_n$$

It is well known that the energy density at arbitrary point A(x_a, y_a, z_a) of the receiver is determined by integration over the last reflecting surface according to the formula [23]:

$$E = \int_\omega B d_{\omega_z} = \int_\omega B \frac{dS\left(\vec{N_m}\,\overrightarrow{MA}\right)}{MA^4}\left(\overrightarrow{MA} \cdot \vec{N_A}\right) \tag{1}$$

where $\vec{N_m}$, normal to the surface at point M; dS, elementary area around point M; $\vec{N_A}$, normal of the receiving surface; B, energetical brightness in a reflected beam.

A generalized approach for determining B is presented in [23].

Integration boundaries in this formula are determined by the coordinate of the heliostat center position, direction of the reflected beams $\vec{K}$, and asimuthal and local angles A_n and h_n, which determine the heliostat's orientation.

As it is known in large-scale MCS, usually each heliostat illuminates the particular target area on the concentrator at the given moment [13]. It is easy to see that in the case of rectangle heliostat, the projection of its borders onto the concentrator midship section (a projection of concentrator surface into XY plane) will be different ellipses. Determination of the integration boundaries is a rather difficult problem due to complicated shapes. That is why it is desirable to move to the coordinate

system connected with the particular heliostat. In this case the integrating boundaries will coincide with the heliostat borders.

Let us determine the Jacobian of this transformation. The origin of the new system **O** is placed at the heliostat's center; axes OX_1 and OY_1 are directed along the height and width correspondingly and the OZ_1 axis along the heliostat's normal. To determine the Jacobian transformation, we apply geometrical definitions. Consider elementary area dS on the surface of the paraboloidal concentrator. For the normal $\vec{N}_m$ at this point, we have

$$\vec{N}_m = \left(\frac{-x}{\sqrt{x^2+y^2+p^2}}, \frac{-y}{\sqrt{x^2+y^2+p^2}}, \frac{p}{\sqrt{x^2+y^2+p^2}} \right)$$

where p is the focal parameter of the paraboloid.

A projection of the elementary surface on dS along the direction of the vector $\vec{K}$ at this point will be equal to

$$dS_K = \frac{dS}{\vec{N}_m \vec{K}}$$

In its turn a projection of this area onto the heliostat surface is determined from the expression

$$dS_g = dx_1 dy_1 = \frac{dS_K}{\vec{N}_g \, \vec{K}} = \frac{dS}{\left(\vec{N}_g \, \vec{K} \right) \left(\vec{N}_m \, \vec{K} \right)}$$

On the other hand, the projection of the elementary area onto the midship section of the concentrator dS_m has the form

$$dS_m = dx\,dy = \frac{dS}{N_{mz}}$$

From these relations we obtain the following expression for the Jacobian transformation:

$$D = \left| \frac{dS_m}{dS_g} \right| = \left| \frac{\left(\vec{N}_g \, \vec{K} \right) \left(\vec{N}_m \, \vec{K} \right)}{N_{mz}} \right| \tag{2}$$

We note that the above presented vector expressions are written taking into account unit normal of the vectors $\vec{N}_g$, $\vec{N}_m$ and $\vec{K}$. Substituting explicit expressions for these vectors into the last formula, finally we get

$$D = \left| \frac{\left(xK_x + yK_y + pK_z \right)\left(K_x \sin h_n + K_y \cos h_n \cos A_n + K_z \cos h_n \sin A_n \right)}{p} \right|$$

For the particular case, when $\vec{K}(0,0,1)$ we obtain obvious formula

$$D = |\cos h_n \cos A_n|$$

Below we apply the developed approach to calculation of energetical brightness at given point of the receiver taking into account errors of reflecting surfaces, shadowing and blocking effects, etc.

At first the relation between the new and old variables should be determined. Let us consider point G with coordinates $(x_1, y_1, 0)$ on the heliostat's reference frame. Transformation of this point into the other reference frame FXYZ is performed by the following expression:

$$\begin{pmatrix} x_f \\ y_f \\ z_f \end{pmatrix} = T_1(A_n)\, T_2(-h_n) \begin{pmatrix} x_1 \\ y_1 \\ 0 \end{pmatrix} + \begin{pmatrix} x_0 \\ y_0 \\ z_0 \end{pmatrix}$$

where T_1 and T_2 are anticlockwise rotation matrixes around X and Y axes, respectively [30], and (x_0, y_0, z_0) are the coordinates of the heliostat's center in the FXYZ frame. Now we have to find the intersection point of the vector $\vec{K}$ with the surface of the paraboloid, i.e., solve the following set of equations

$$\left. \begin{aligned} \frac{x - x_f}{K_x} &= \frac{y - y_f}{K_y} = \frac{z - z_f}{K_z} \\ x^2 + y^2 &- p^2 + 2pz = 0 \end{aligned} \right\}$$

from which we obtain

$$x = x_f + tK_x, \quad y = y_f + tK_y, \quad z = z_f + tK_z,$$

where

$$t = \frac{-b + \sqrt{b^2 - ac}}{a}, a = K_x^2 + K_y^2, b = x_f K_x + y_f K_y + pK_z, c = x_f^2 + y_f^2 - 2p z_f$$

Exposure B at the given target point A is determined by the inverse ray tracing method when a ray is directed from this point to the current point M on the concentrator, then a normal to the reflecting surface at this point is determined, and the ray reflected in the heliostat's direction is found. After that the crossing point of this ray with the given heliostat's reflective surface and the corresponding normal at this point is determined. Finally, the direction of the last reflected ray is found, and depending on the fact, whether this ray hits solar disk (determine the angle φ) or not ($B = 0$), the energetical brightness is determined. Distribution of the brightness over the solar disk is taken into consideration according to the Jose formula [23]:

$$B(\varphi) = 1.23 \frac{E_0}{\pi \varphi_0} \cdot \frac{1 + 1.5641\sqrt{1 - \frac{\sin^2(\varphi)}{\sin^2(\varphi_0)}}}{2.5641},$$

where φ_0 is the apparent angular size of the solar disk (16 min) and E_0 is the solar radiation.

During the ray tracing procedure, shadowing and blocking conditions of the given heliostat by other heliostats, technological tower, and other installations are taken into account.

The real normal is given with reference to the vector $\vec{N}_m$. For this purpose an auxiliary Cartesian reference frame $X^1Y^1Z^1$ is introduced with the origin at point M and Z axis, directed along the vector $\vec{N}_m$, i.e.,

$$\vec{L}_3 = (L_{3x}, L_{3y}, L_{3z}) = \vec{N}_m \ (N_{mx}, N_{my}, N_{mz}),$$

where $\left(\vec{L}_1, \vec{L}_2, \vec{L}_3\right)$ are directing unit vectors

The direction of unit vectors may be chosen in different ways, depending on the character of deviation of the real vector from the ideal one. Let the unit vectors lay on the meridional and sagittal sections. In this case the unit vectors $\vec{L}_1$ and $\vec{L}_2$ can be determined via the vector product of previously determined vectors:

$$\vec{L}_2 \ (L_{2x}, l_{2y}, L_{2z}) = \vec{L}_3 \times (0, 0, -1) = \frac{(-L_{3y}, L_{3x}, 0)}{\sqrt{L_{3x}^2 + L_{3y}^2}}$$

Now, the unit vector $\vec{L}_1$ can be determined using $\vec{L}_2$ and $\vec{L}_3$:

$$\vec{L}_1 = \vec{L}_2 \times \vec{L}_3 = \frac{\left[L_{3x}L_{3z}, L_{3z}L_{3y}, -\left(L_{3x}^2 + L_{3y}^2\right)\right]}{\sqrt{L_{3x}^2 + L_{3y}^2}}$$

The angle between the ideal direction $\vec{N}_m$ and real normal γ, which characterizes angle errors of the surface, is unambiguously determined by two angles μ and ν, which are actually its projections onto two mutually orthogonal planes, for example, meridional and sagittal planes [23]. It is easy to see that the angle γ is determined via μ and ν, according to the following relation:

$$tg^2\gamma = tg^2\mu + tg^2\nu \tag{3}$$

Or if smallness of angles μ and ν is taken into account

$$\gamma \cong \sqrt{\mu^2 + \nu^2} \tag{4}$$

Now the following expression may be written for components of the real normal:

$$N_{xr} = \cos\gamma \ tg\mu, \quad N_{yr} = \cos\gamma \ tg\nu, \quad N_{zr} = \cos\gamma$$

Error density distribution of BSF reflecting surfaces for angles μ and ν can be determinate by experiments. Here we supposed that these errors are to be distributed according to the Gaussian function. For a set of random values μ and ν, individually having Gaussian distribution with zero mean, a two-dimensional probability distribution in the absence of correlations has the form [31].

$$W(\mu, \nu) = \frac{1}{2\pi\sigma_\mu\sigma_\nu} \ \exp\left[-\frac{1}{2}\left(\frac{\mu^2}{\sigma_\mu^2} + \frac{\nu^2}{\sigma_\nu^2}\right)\right] \tag{5}$$

where σ_μ^2, σ_ν^2 are dispersions of corresponding random values.

Generation of random numbers with a given distribution function is the special issue. To obtain pseudorandom numbers with Gaussian distribution function, we used (after thorough testing) the following expression:

$$\xi = a + \sigma \left[\sin \left(2\pi\eta_1 \right) \sqrt{-2\ln \left(\eta_2 \right)} \right]$$

where η_1 and η_2 are random numbers uniformly distributed over the interval [0:1]. Note that high-level programming languages have such built-in functions.

Note that in the case of Rayleigh distribution, i.e., when $\sigma_\mu = \sigma_\nu = \sigma$, an explicit expression for the distribution density (Eq. (5)) may be derived. Omitting simple transformations we obtain the following result:

$$W(\gamma) = \frac{\gamma}{\sigma^2} \exp \left(-\frac{\gamma^2}{2\sigma^2} \right), \quad \gamma > 0 \tag{6}$$

as this takes place

$$\sigma_\gamma = \sqrt{D\gamma} = \sigma\sqrt{2}$$

So, the distribution for deviations of the angle γ does not obey the Gaussian law. Experimental results obtained for mirrors of the BSF also indicate the non-Gaussian character of error distributions.

Now the vector $\vec{N}_r$ must be transformed to the basic reference frame:

$$N_{mx} = L_{1x}N_{xr} + L_{2x}N_{yr} + L_{3x}N_{zr}, \quad N_{my} = L_{1y}N_{xr} + L_{2y}N_{yr} + L_{3y}N_{zr},$$

$$N_{mz} = L_{1z}N_{xr} + L_{2z}N_{yr} + L_{3z}N_{zr}$$

Real normals for other reflecting parts may be determined in the same way. In the case when total errors have distribution law distinct from Gaussian, direction of the real normal can be determined using the error density distribution function [31].

It should be emphasized that in view of the character of the integrand function, chosen approach to solution of the problem, specific features of the algorithm, and possibilities of modern computers, it is desirable to calculate the integral (Eq.(1)) by the statistical method (Monte Carlo procedure) [31]. Moreover, in the problem under consideration, simultaneous determination of exposure values is possible in all given target points (not only at one point) using one set of random numbers is possible. In this way calculation steps are significantly reduced.

Corresponding software based on the above described technique has been developed in Delphi programming language. Using these programs case calculations of the BSF energetical characteristics are performed.

5. Characteristic features of the energy modes of the LSF

5.1 Preliminary notes and some assumptions

Analysis of the characteristics of the processing modes of material synthesis and heat treatment, i.e., isochronic maps of the energy density distribution in the focal zone of the LSF, shows that they are very different. When referring to the energy

characteristics of the furnace, it is necessary to consider many factors, which are in a certain temporary state. This is why, when specifically referring to the energy state of the furnace, it is necessary to provide these factors with the corresponding information. Despite this, some characteristic features of the energy parameters of the LSF can be refined, and it is necessary to analyze a large amount of information on the energy density distribution in the focal zone from certain heliostats, shelves, and groups of heliostats for the various system conditions in order to determine them.

The aim of this paragraph is a detailed analysis of the LSF energy characteristics based on numerical calculations. The peculiarities of the methods for calculating the LSF energy characteristics and their implementation for specific problems are given in [25, 28, 29]. Some characteristic features of the LSF energy characteristics are given in these works but with no detailed theoretical or design analysis.

Each heliostat illuminates a certain area of the concentrator in the normal operation mode of the device. A scaled circuit of the concentrator midsection with the block circuits (solid line) and relevant heliostat zones (dotted line) is shown in **Figure 3**. The numbers of the heliostats are given in the left angle of their zone. The upper contour line of the building roof adjacent to the process tower, which insignificantly blocks the light flux from the heliostats, is also shown in **Figure 3**. As is clear from **Figure 3**, the heliostats 55 and 62 are most inefficient (less than 50% of the heliostat area is used).

The LSF energy spot is formed from the energy contributions (irradiance/energy density) of certain heliostats. The energy contributions of the heliostats depend on the place of their location, reflection coefficient, mirror inaccuracy, adjustment state, etc.

The authors developed a program to calculate the energy characteristics taking into account the real influencing factors in order to study the peculiarities of the LSF energy characteristics [25]. The program uses Monte Carlo method to calculate
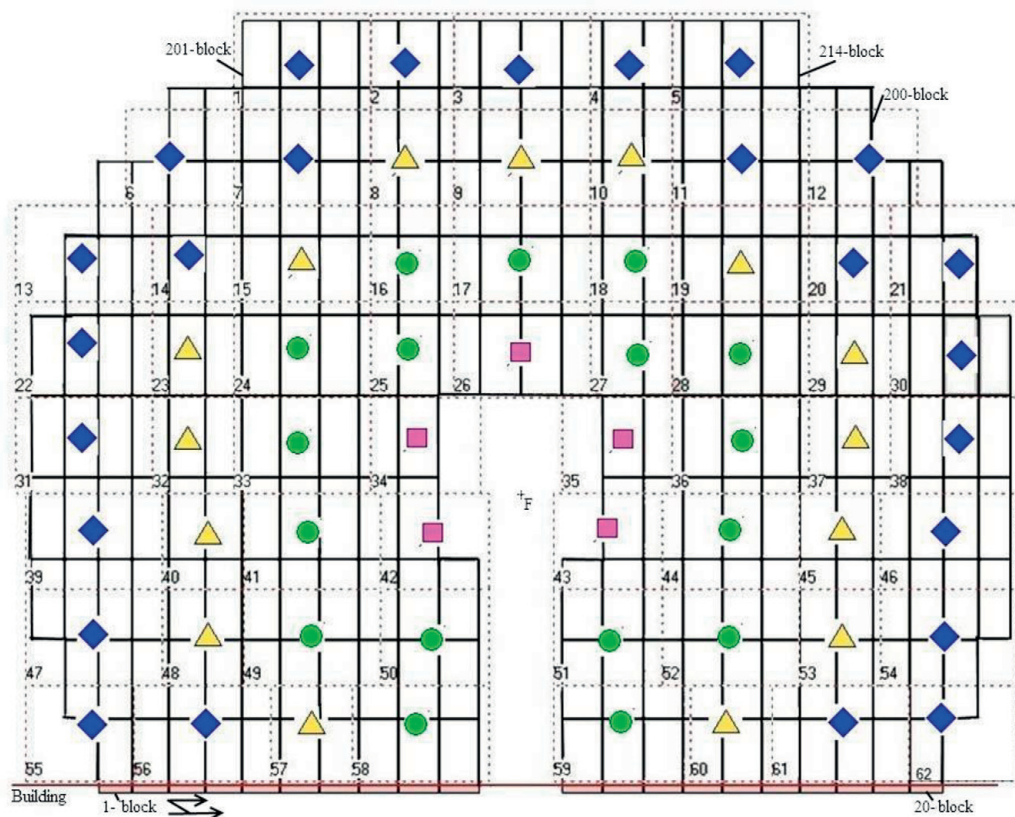

Figure 3.
Midsection of concentrator of blocks of facets and corresponding zones of heliostats.

the integral. Comparative analysis of the calculation results shows that the calculation accuracy is 2–4%. The intensity of the solar beam is determined by backtracking of the beam path. The program interface is shown in **Figure 4**, along with the layout of the heliostats and numbers of the heliostats of certain shelves.

The input parameters of the program are the beam solar radiation E_0 [W/cm^2]; R_{sc} and R_{sg} are the reflection coefficients of the mirrors of the concentrators and heliostats, the root-mean-square mirror inaccuracy of the heliostats σ_g and concentrator σ_c, the relative boundaries of integration of the heliostats, the number of points in the focal plane, the number of playouts in the Monte Carlo method, etc. The energy density distribution was determined for a flat receiver located in the focal plane of the concentrator in all calculations.

In the solar energy problems, the reflecting properties of the real mirror are characterized by the root-mean-square angular inaccuracy σ defined as a root-mean-square value of deviations of the real normal from the ideal (γ). It is assumed in many calculations that the meridional (μ) and sagittal (ν) components of the angle of deviation from the normal ($\gamma^2 \approx \mu^2 + \nu^2$) obey a Gaussian law for integral paraboloid concentrators [23]. The sagittal component of deviation ν is often neglected. However, in the case of the LSF, due to the large sizes of the device, the curvature of some concentrator facets (with dimensions of 45 × 45 cm in various sections), especially the peripheral facets, is very similar and small; i.e., the facets are almost isotropic reflectors. The reflecting surfaces of the heliostats also consist of flat reflectors. For this reason, it is assumed in calculations that the probability distribution of the deviation of the mirror normal γ obeys a Gaussian law with dispersion σ. In other words, if the direction of the real normal relative to the ideal is expressed by the formula

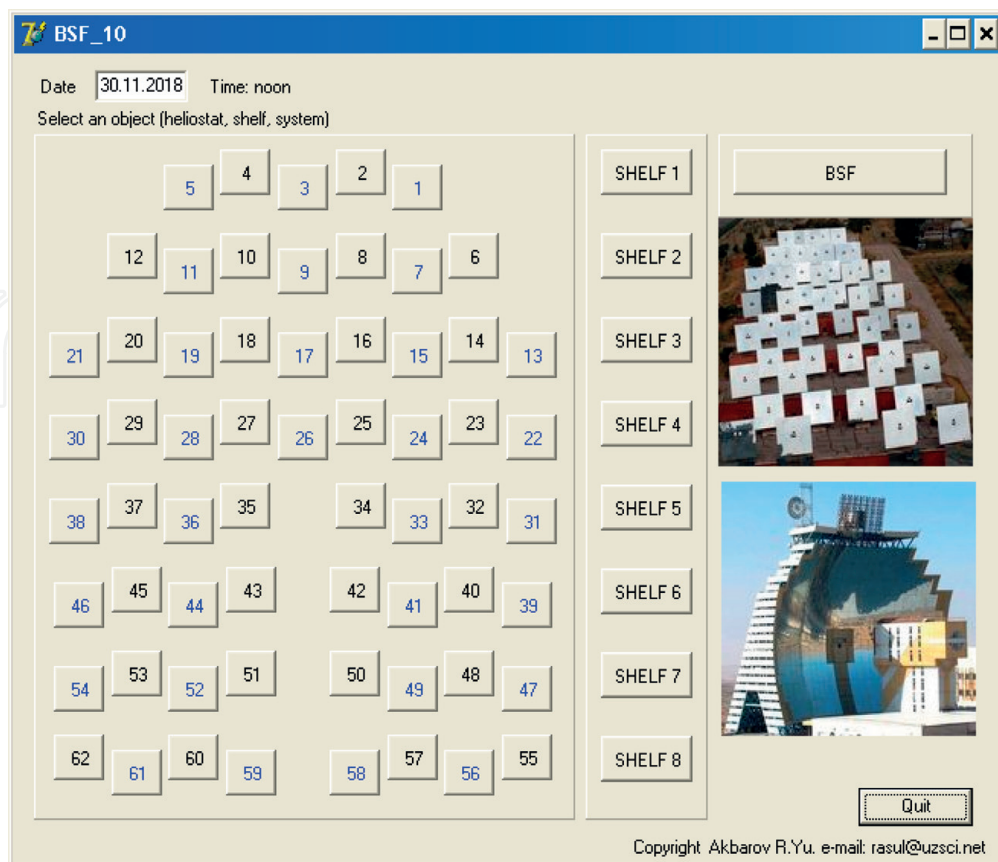$$l_x = \sin\gamma\cos\varphi, \quad l_y = \sin\gamma\sin\varphi, \quad l_z = \cos\gamma,$$

Figure 4.
Program interface.

γ varies according to a Gaussian law with dispersion σ, and φ varies uniformly within 0–2π.

This program was used to carry out some sequences of the numerical calculation to determine the irradiance distribution (energy density) of certain heliostats, shelves of heliostats, groups of heliostats, and the entire LSF with different inaccuracies of the reflecting surfaces of the heliostats and concentrator (1–10 angular minutes).

5.2 Analysis of the results of numerical calculations

5.2.1 Analysis of the energy characteristics of the whole system

The scope of calculations is quite large, which is why some peculiarities of the LSF energy characteristics are revealed from analysis of data, which are given below.

Figure 5a shows the dependence of the focal irradiance E_F on the mirror inaccuracy of the heliostats σ_g and concentrator σ_c (E_0 = 700 W/m^2, $R_{sc} = R_{sg}$ = 0.6).

The mirror inaccuracies of the heliostats σ_g are measured on the horizontal axis. Some individual lines correspond to various inaccuracies of the concentrator mirrors σ_c. It is easy to see that the change in focal irradiance is expectedly more sensitive to mirror inaccuracies of the concentrator than the heliostats. However, beginning with 2.5–3.0 angular minutes, the influence of the mirror inaccuracies of the heliostats and concentrator on the character of the irradiance distribution does not significantly differ and is approximately similar. In practice, we have the mirror inaccuracies within 3–10 angular minutes. This is why, for decreasing (by an order of magnitude) calculation variants, it is assumed that the mirror inaccuracies of the heliostats and concentrator are similar ($\sigma_c = \sigma_g = \sigma$). As mentioned above, it is considered that these mirror inaccuracies obey a normal law of errors. Under such an assumption, the dependence of the focal irradiance of the LSF on the mirror inaccuracy will be a function of one variable, which can be represented as the following empirical formula:

$$E_F = \frac{43578 E_0 R_{sc} R_{sg}}{1 - 0.034\sigma + 0.028\sigma^2} \left[\frac{W}{cm^2}\right]$$

where σ is the root-mean-square mirror inaccuracy per minute. The relative error of this formula is no more than 1.2%. A diagram of this dependence is shown in **Figure 5b**.

Let us consider the size of the focal spot in different cases. Usually, the value where the irradiance is 10% of the focal irradiance is selected as the size of the focal spot in solar concentrators. In the case of the LSF, for descriptive reasons and convenience of analysis, various levels of irradiance within 3–11 W/cm^2 were used as the contour (isometric) line of the focal spot. The contour lines of the focal spot for various mirror inaccuracies (E_0 = 700 W/m^2, $R_{sc} = R_{sg}$ = 0.6) are shown in **Figure 6**.

A certain idea of the character of the irradiance distribution for various mirror inaccuracies can be obtained from this, taking into account the value E_F from **Figure 5b**. It can be seen that the shape of the focal spot is not round, but a bit prolate along the horizontal axis. This is evidently related to the shape of the midsection of the concentrator. It can be also seen from **Figure 5b** that beginning from the second or third minute of the mirror inaccuracy, the character of the energy distribution (extension of the spot contour line) varies gradually and relatively uniformly as a function of σ.
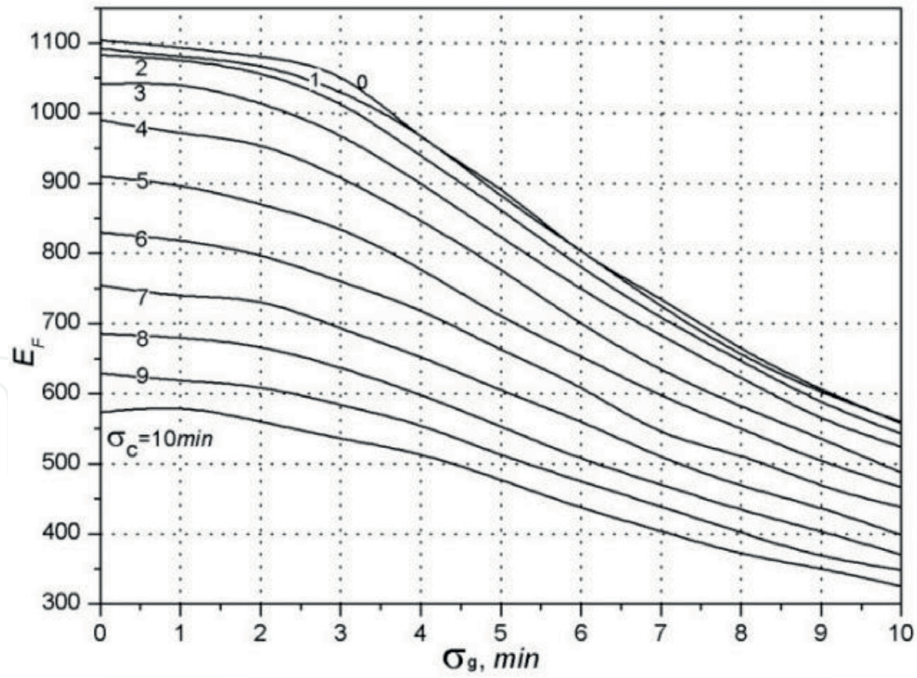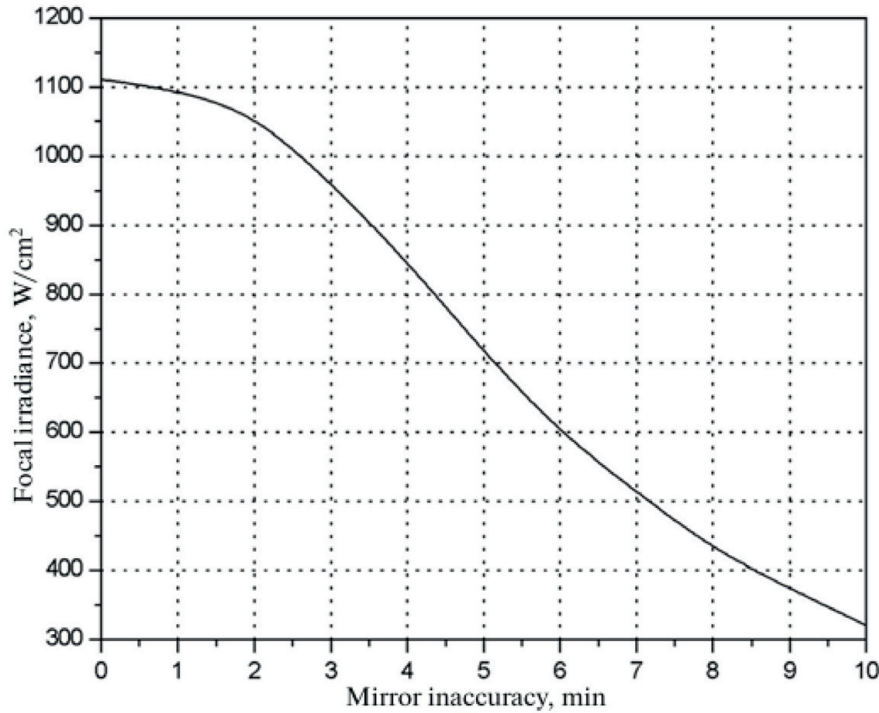
Figure 5.
(a) Dependence of focal irradiance E_F on the mirror inaccuracy of the heliostats σ_g and concentrator σ_c and (b) dependence of focal irradiance E_F on the mirror inaccuracy (case $\sigma_g = \sigma_c$).

Thus, as follows from the given analysis and without violating the generality of the results, the characeristic parameters of the LSP can be calculated, and its energy characteristics can be analyzed on their basis. On the basis of this data, the energy characteristics of the furnace can also be estimated for its other parameters. The following values were used as the characteristic parameters of the LSF: $E_0 = 700$ W/m^2 is the beam solar radiation, and $R_{sc} = R_{sg} = 0.6$ is the reflection coefficient of the mirrors of the concentrator and heliostats; the mirror inaccuracies of the concentrator and heliostats are $\sigma = 7$ ($\sigma = \sigma_c = \sigma_g$) angular minutes.
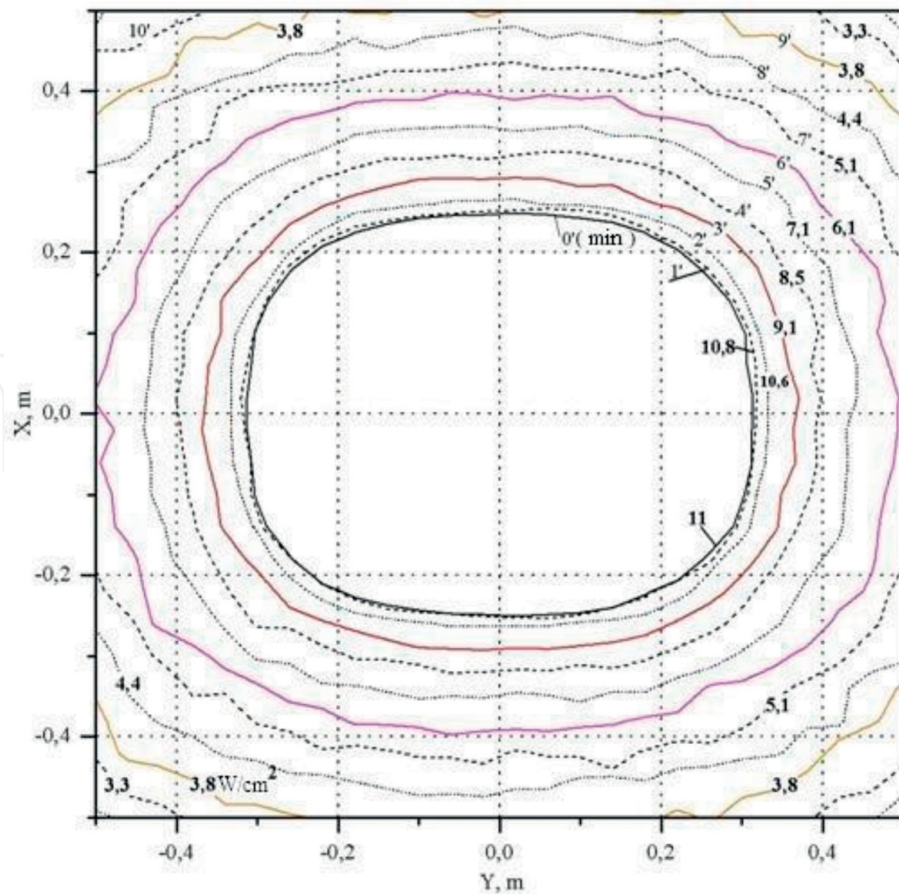
Figure 6.
Contour lines of focal spot.

Figure 7 shows the dependence (in the section) of the irradiance distribution in the focal zone of the LSF for the specified parameters with various inaccuracies of the reflecting mirrors.

Figure 8 shows the energy density distribution in the focal zone of the LSF in the form of isometric lines with equal irradiances and its three-dimensional
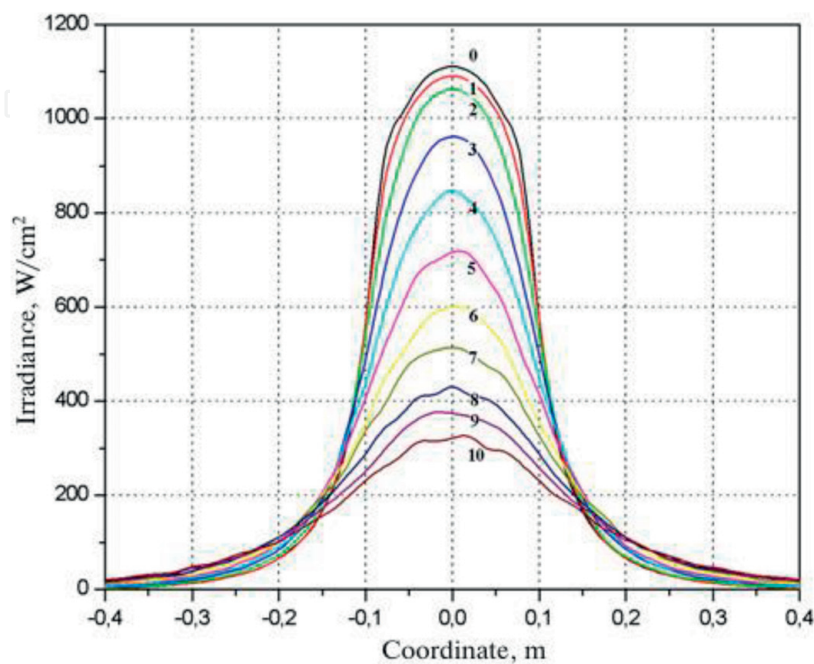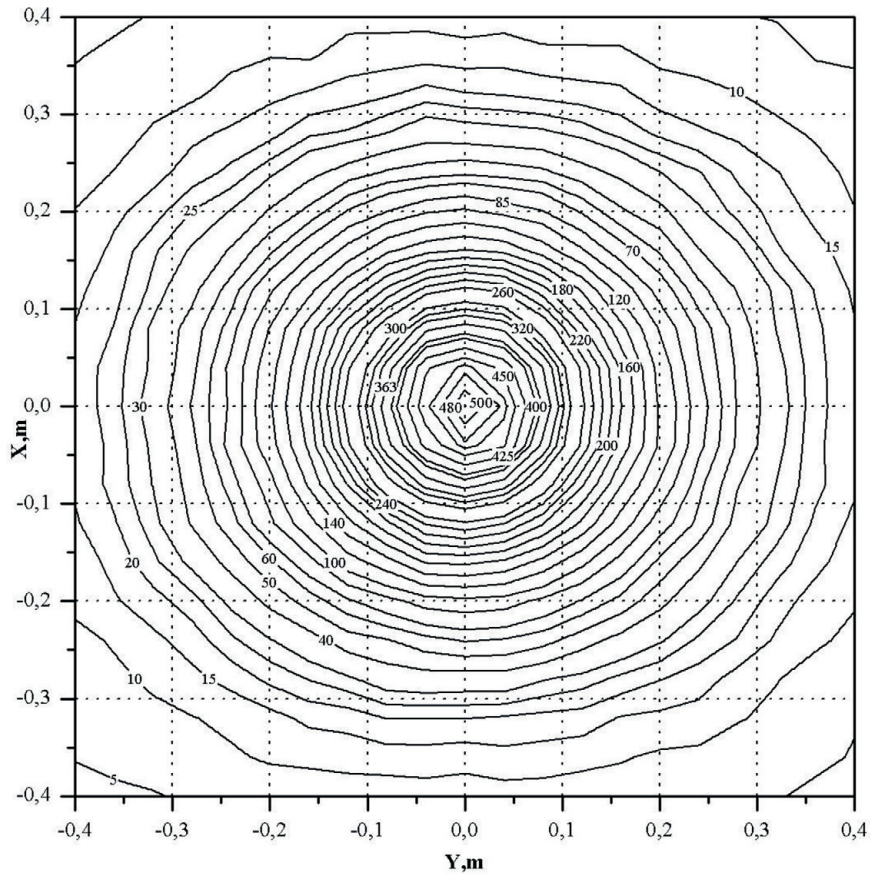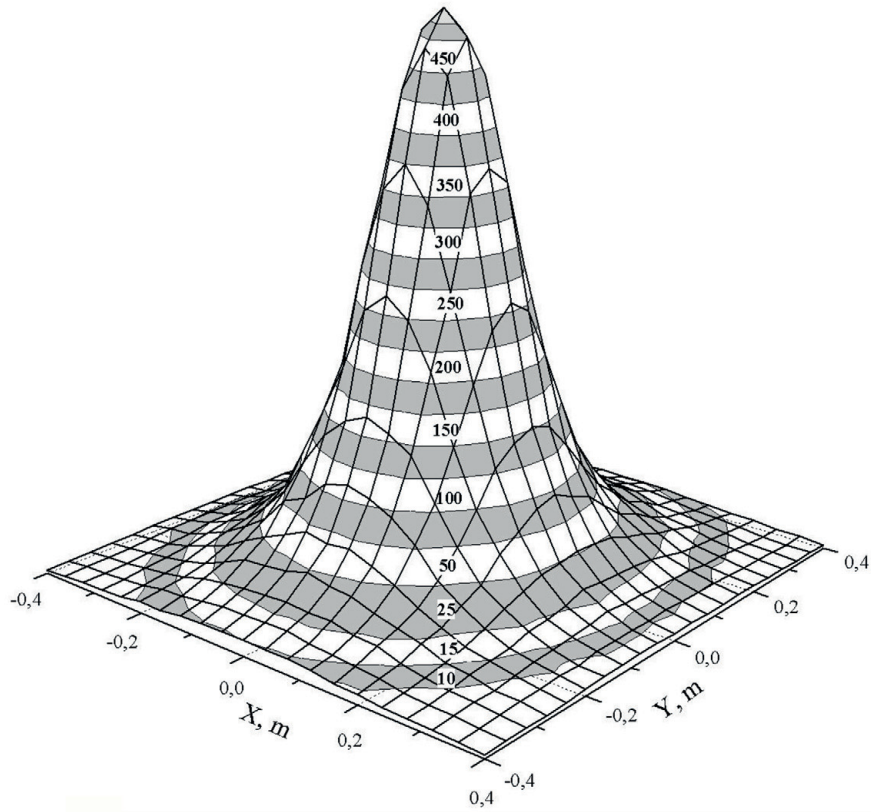

Figure 7.
Irradiance distribution in the section of focal zone of LSF.

Figure 8.
(a) Energy density distribution from total system (isometric lines) and (b) energy density distribution from total system (three-dimensional).

representation specifying the irradiance levels. The maximum energy density at the center of the spot is 506 W/cm^2. The asymmetry of the focal spot can be also seen in the quantitative measures in **Figure 8**.

It should be noted that the furnace power in the selected parameters has a value of W_0 = 0.6•0.6•700 W/m^2•1906m^2 = 480.3кW. To check the correctness of the calculations, the amount of light energy per unit time (power) arriving at the focal zone of the LSF is determined in all calculations, and it was compared to the W_o value. It turned out that the difference between these values does not exceed 2–3%.

5.2.2 Representation of the calculated data by empirical formulas

Calculations are carried out to select the empirical formulas for the best approximation of the two-dimensional calculated data. The selection of the different types of functions shows that for this purpose, a two-dimensional Gaussian function (with six parameters) gives the best fit, which is given by

$$E(x,y) = E_0 + A \, \exp\left\{ -\frac{1}{2}\left(\frac{x - x_c}{w_x}\right)^2 - \frac{1}{2}\left(\frac{y - y_c}{w_y}\right)^2 \right\} \tag{7}$$

The LSF conditions with various inaccuracies of the reflecting mirrors are considered, and the parameters of the empirical formulas and standard root-mean-square deviations of irradiance are determined for each case according to the following formula:

$$E_\sigma = \sqrt{\frac{\sum_{i=1}^{N}\left(E_i - E(x_i, y_i)\right)^2}{N}}$$

where i is number of the current points, E_i is the calculated data, and N is point number, in our case, 2601. **Table 1** gives the determined parameters of the two-dimensional Gaussian functions and E_σ values for the various mirror inaccuracies of the heliostats and concentrator.

It is clear from **Table 1** that with an increase in mirror inaccuracies, the empirical formulas describe the calculated data better. Despite this, when using these formulas, it is necessary to make certain in each case that it is possible to use them. It should be noted that in all cases, the total power of the focal spot determined using the empirical formulas almost coincides with the power value determined by the calculated data. It also should be mentioned that in all cases, the sum of

σ, мин	E_0	A	x_c	w_x	y_c	w_y	E_σ
$\sigma_c = \sigma_g = 2$	4.71	1164.28	0.00006	0.074	0.00014	0.079	12.25
$\sigma_c = \sigma_g = 4$	7.02	840.87	0.000095	0.084	−0.00022	0.09	8.21
$\sigma_c = \sigma_g = 7$	9.24	474.82	−0.00031	0.106	0.00015	0.115	7.34
$\sigma_c = \sigma_g = 10$	10.53	290.26	0.0004	0.129	0.00058	0.139	6.10
$\sigma_c = \sigma_g = 12$	11.03	217.65	0.00056	0.143	0.00031	0.155	5.35
$\sigma_c = 7, \sigma_g = 5$	8.79	572.7	0.00054	0.098	0.0004	0.106	7.97
$\sigma_c = 7, \sigma_g = 4$	8.58	624.0	0.00039	0.094	0.000024	0.102	8.21
$\sigma_c = 5, \sigma_g = 3$	7.24	841.64	0.00031	0.084	−0.00012	0.09	8.42

Table 1.
Parameters of empirical formulas.

$(E_i - E(x_i, y_i))$ over all points is approximately zero. The empirical formulas were determined using the OriginPro8 graphics package (www.originLab.com).

5.2.3 Analysis of the power characteristics of the focal spot and average concentration

The value of the spot power and average radiation concentration in certain zones of the focal spot is important for some problems. The spot powers W in different square zones with the center at the focus of the concentrator (d is zone diameter) and average radiation concentrations E_{aver} in these zones are determined (**Figure 9**).

5.2.4 Analysis of the energy characteristics of certain LSF shelves

The energy characteristics of certain LSF shelves are also studied.

The three-dimensional irradiance distributions of certain shelves of heliostats are given for comparative analysis in **Figure 10**. The irradiance levels are specified in the belt lines. It is clear from **Figure 10** that the contribution of shelf 1 is the smallest from the viewpoint of the maximum irradiance, and the spot is more prolate along the X axis (vertically). The irradiance distributions from shelves 2, 3, and 8 have an approximately round symmetry. It is also seen that the focal spot of shelves 4, 5, 6, and 7 is more prolate along the Y axis (horizontally). The focal irradiance is maximum for shelf 4. The vertical section of the irradiance distribution from certain shelves is shown in **Figure 11**. The maximum values of irradiance by the heliostat shelves are as follows: 19, 41, 69, 93, 80, 80, 72, and 52 W/cm^2, and their sum is 506 W/cm^2. The quantitative characteristics of the irradiance distribution of certain shelves can be determined from the diagram.

Note that inclusion or exclusion of some individual shelves of heliostats in the tracking mode allows a certain set of possible irradiance distributions to be obtained. It is easy to see that the number of variants of inclusion/exclusion of the heliostat shelves N_p is 256. Actually,

$$N_p = \sum_{k=0}^{8} C_8^k = \sum_{k=0}^{8} \frac{8!}{(8-k)!k!} = (1 + 8 + 28 + 56 + 70 + 56 + 28 + 8 + 1) = 256$$
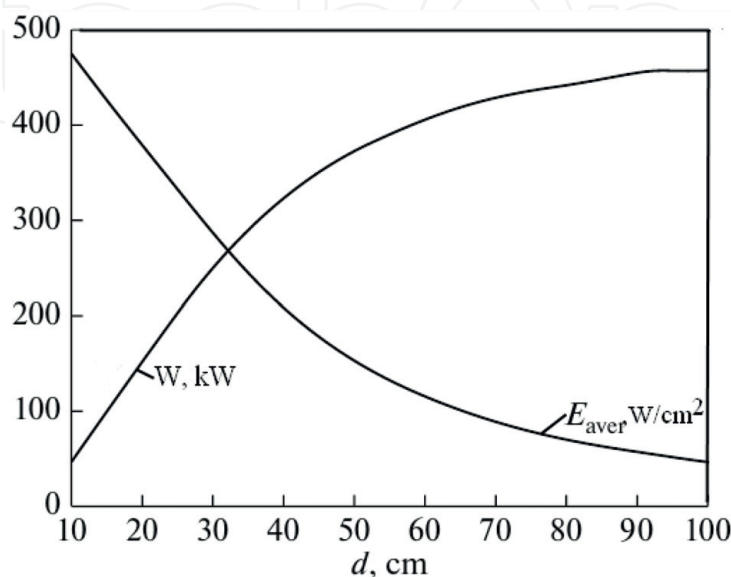

Figure 9.
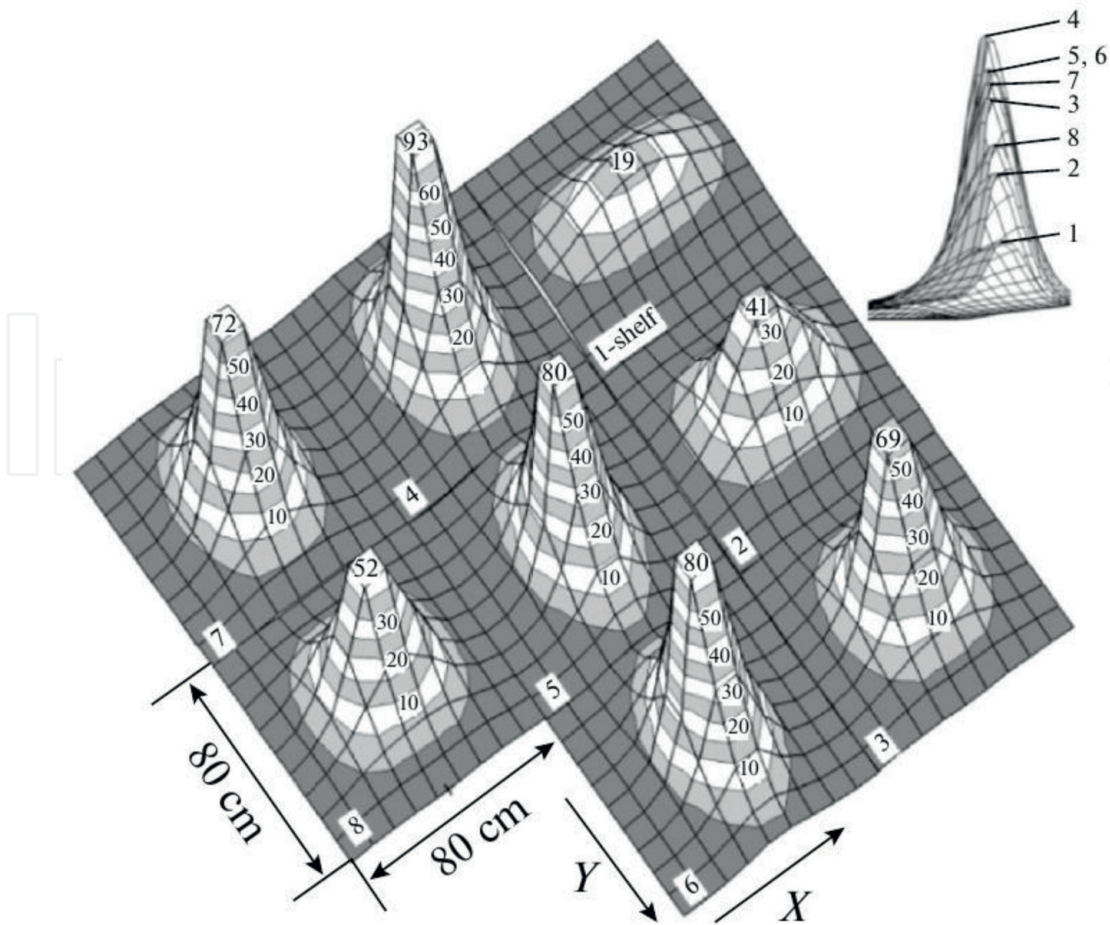*Power and average concentration in different zones of focal spot.*

Figure 10.
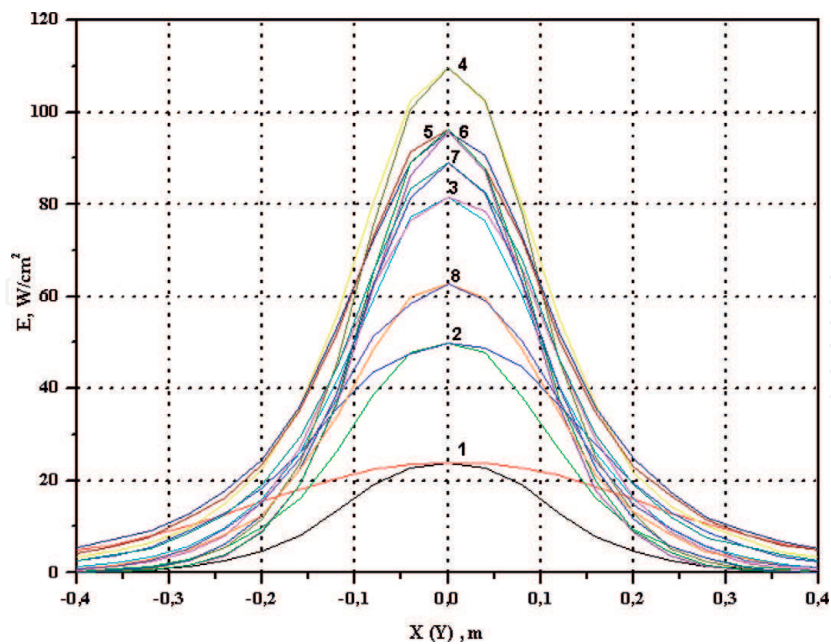*Three-dimensional energy density distribution from certain shelves of LSF heliostats.*

Figure 11.
Energy density distribution from certain shelves of LSF heliostats.

Figure 12 shows the dependence of the maximum irradiance (points in the diagram) of the distribution on the number *N* of the variant of inclusion/exclusion of the heliostat shelves. For example, the entry 01111111 means that all shelves except for first are engaged. Transfer from the number of the variant *N* to such a type of the entry is as follows: *N* is converted to the binary representation, and the
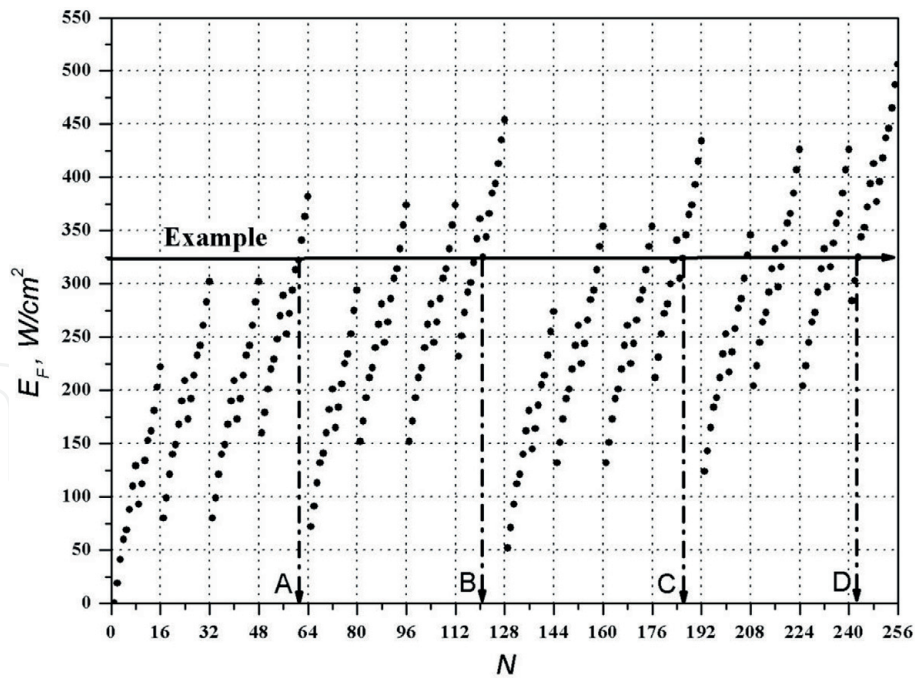
Figure 12.
Variants of inclusion/exclusion of shelves of LSF heliostats.

obtained number is read in reverse order. For example, 254_{10} = 11111110_2, and the entry (combination) has the form 01111111. In the figure, the line *Example* corresponds to the required maximum density 325 W/cm^2, and such energy density is achieved using four variants: A, B, C, and D.

5.2.5 Heliostat rearrangement and its energy characteristics

Let us consider the energy characteristics of certain heliostats of the LSE. The focal irradiances and character of irradiance distribution of the heliostats significantly differ from each other. Analysis of the calculation results showed that the relative focal irradiance (normalized to the focal irradiance of the LSF) of the heliostats varies insignificantly with various mirror inaccuracies. In **Table 2**, this data is presented for 33 heliostats, taking symmetry into account.

Note that the maximum contribution of the heliostat to the focal irradiance is higher when the center of the heliostat is closer to the optical axis of the concentrator. This is why the heliostats can be grouped according to this principle. It can be expected that the shape of the focal spot of certain groups will be more symmetric.

No.	%	No.	%	No.	%	No.	%	No.	%
1	0.67	2	0.56	3	1.05	6	0.45	7	1.38
8	1.12	9	2.06	13	0.44	14	0.79	15	2.18
16	1.74	17	3.21	22	0.79	23	1.04	24	2.96
25	2.41	26	4.34	31	0.93	32	1.2	33	3.45
34	2.25	39	1.02	40	0.97	41	3.39	42	2.17
47	0.8	48	1.04	49	2.96	50	2.34	55	0.25
56	1.31	57	1.24	58	2.55				

Table 2.
The relative focal irradiance of the heliostats.

Based on the analysis of illumination of the concentrator by the heliostats, four groups of heliostats are distinguished. The heliostats with a close distance from the optical axis of the concentrator are combined in each group. The numbers of heliostats in these groups are as follows:

Group 1: 26, 34, 35, 42, 43, and 5 heliostats (1–5, rectangle).

Group 2: 16, 17, 18, 24, 25, 27, 28, 33, 36, 41, 44, 49, 50, 51, 52, 58, 59, and 17 heliostats (6–22, circles).

Group 3: 8, 9, 10, 15, 19, 23, 29, 32, 37, 40, 45, 48, 53, 57, 60, and 15 heliostats (23–37, triangles).

Group 4: 1, 2, 3, 4, 5, 6, 7, 11, 12, 13, 14, 20, 21, 22, 30, 31, 38, 39, 46, 47, 54, 55, 56, 61, 62, and 25 heliostats (38–62, rhombs).

The new number of the heliostats is given in brackets. In **Figure 3**, heliostats belonging to one group are designated, respectively, by rectangles, triangles, circles, and rhombs. As the analysis of the numerical calculations has shown, the shape of the focal spot of certain groups of heliostats is almost symmetric, except for group 4, where a slight asymmetry is observed. This is why the energy density distributions from certain groups in the horizontal section (Y axis) are shown in **Figure 13**.

In the general case, to determine the necessary possible focal irradiance (or the required irradiance), it suffices to construct a diagram of the dependence of the cumulative sum of the focal irradiance on the number of the heliostat, i.e.,

$$y(n) = \sum_{i=1}^{i=n} E_F(i), \quad n = 1 - 62$$

This diagram is similar to that in **Figure 12** in the character of construction; only the new numbers of heliostats are measured on the horizontal axis. A diagram of function $y(n)$ for such a new group of heliostats is shown in **Figure 14**.

5.2.6 Analysis of the focal spot of the individual heliostats

The authors performed a comparative analysis of the energy density distributions from certain heliostats. The focal irradiances of certain heliostats can be determined from **Table 2**, knowing the total focal irradiance of the LSF, 506 W/m^2. The isometric line corresponding to a value of 1 W/cm^2 is selected from the
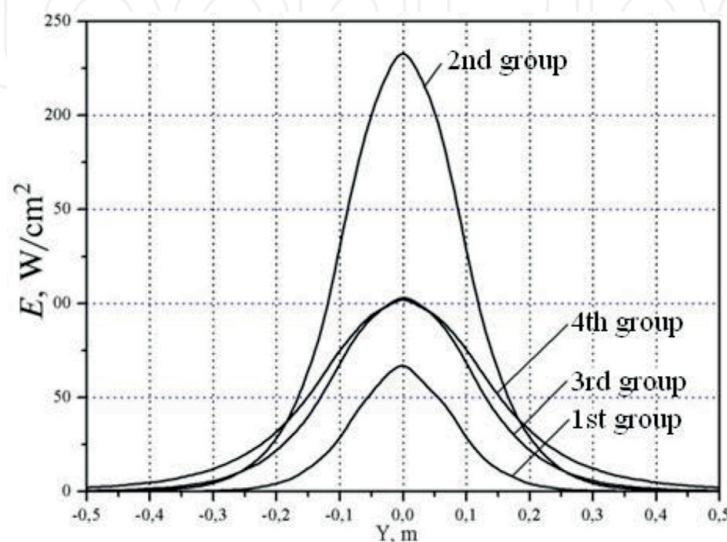

Figure 13.
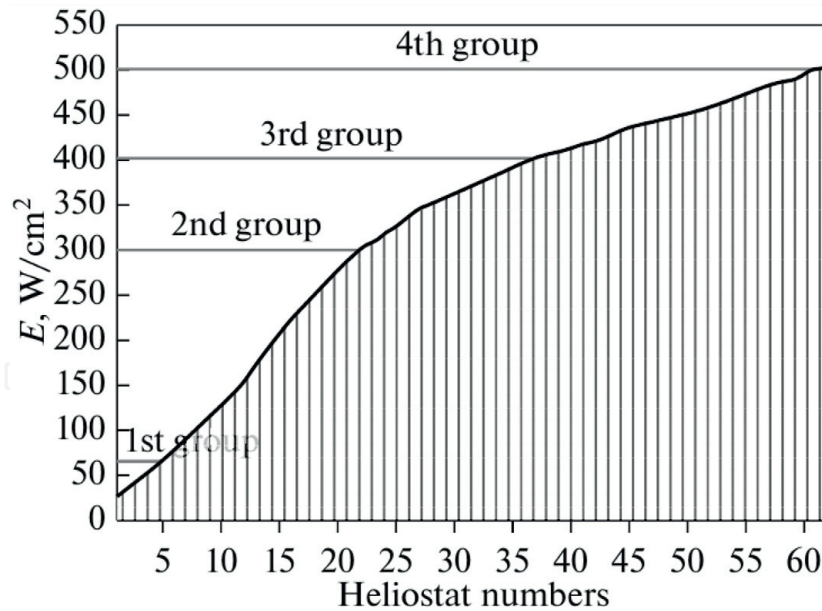*Energy density distribution from certain groups of heliostats.*

Figure 14.
Increasing energy density from certain groups of heliostats.

two-dimensional diagram of the irradiance distribution from a certain heliostat represented as isometric lines of a similar irradiance. It is clear that this isometric line corresponds to the contour line of the focal spot of the considered heliostat. The contour lines of the spots of certain heliostats (33 heliostats) are shown in **Figure 15a** and **b**. For descriptive reasons, so as not to overload the diagram, the heliostats are conditionally divided into two groups, central (left) and extreme (right). The contour line of the focal spot of the selected heliostat can be accurately traced from the diagram.

The character of the energy density distribution can be estimated if the maximum irradiance and geometry of the focal spot of the heliostat are known.

5.2.7 Analysis of the changes of the energy distribution within a day

One of the most important problems is the change in the focal energy density distribution within a day, occurring due to the daily variation in beam solar radiation. As an example, **Figure 16** shows a diagram characterizing the change in the focal energy density distribution along the horizontal axis of the LSF. For the beam
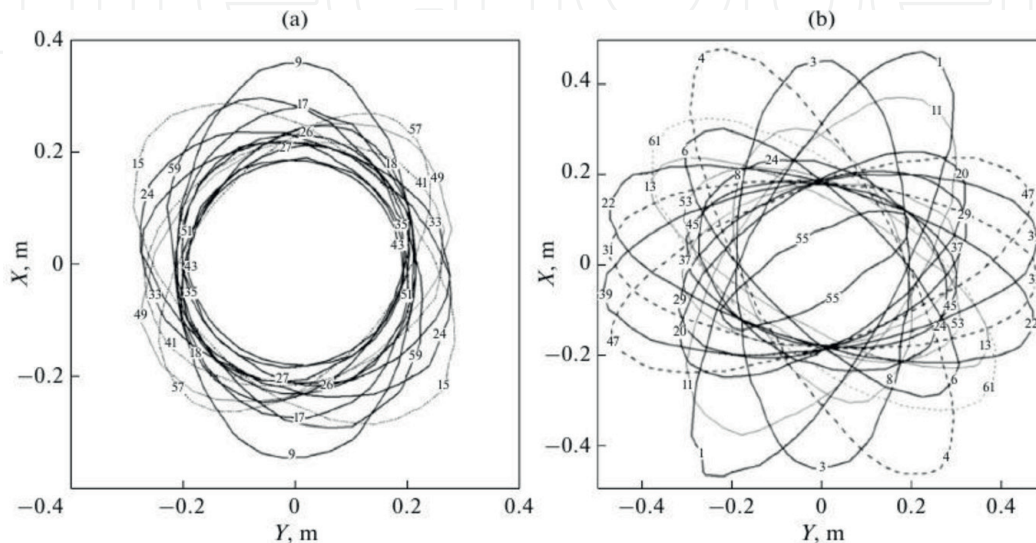

Figure 15.
Contour lines and orientation of focal spots of certain heliostats of LSF (Figures in contours - numbers of heliostats)
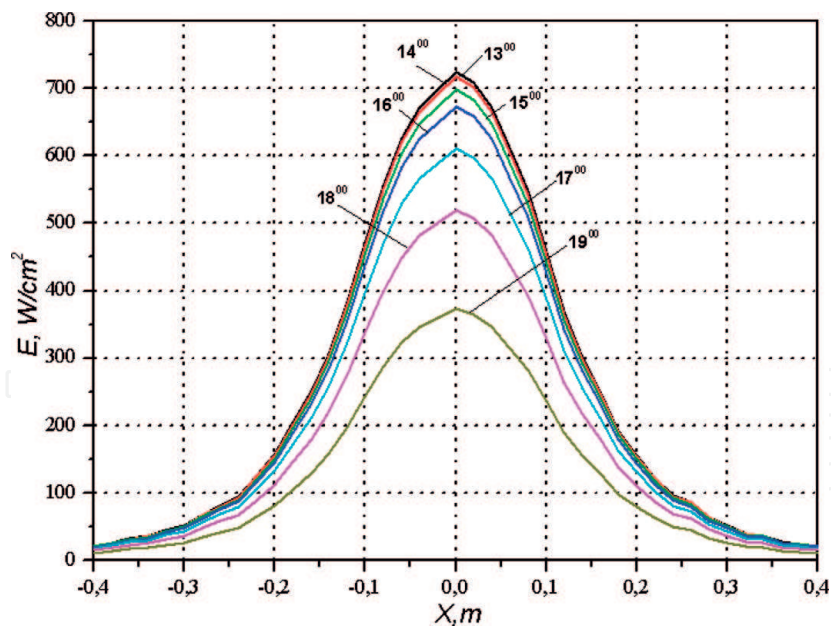
Figure 16.
Variation in energy density within 1 day.

solar radiation, a clear sunny day is selected according to data from the Parkent meteorological station: 18 June 2013. It can be seen from **Figure 16** that within the time interval of 10:00–16:00, i.e., within 6 h (13:00 is approximately midday), the character of the energy density distribution does not change significantly. It should be noted that a similar analysis should be carried out for other periods of time.

6. Conclusion

Let us note, lastly, that the performed theoretical and design analyses of the LSF energy characteristics and their revealed features, general patterns, and presented detailed data allow to correctly determine the configuration parameters of the LSF for various required process modes in the focal zones of the furnace. The long-term experience in application of the LSF for synthesis and thermal processing of various high-temperature materials has shown that the accuracy in implementing certain process modes significantly affects the final characteristics of the product. This is why the obtained results have important practical value for efficient operation of the LSF of the Academy of Sciences of the Republic of Uzbekistan.

Author details

Akbarov Rasul
Institute of Materials Science of the Academy of Sciences of the Republic of
Uzbekistan, Tashkent, Uzbekistan

*Address all correspondence to: aryu12@mail.ru

IntechOpen

References

[1] Rakhimov RK. Synthesis of functional ceramics on the BSP and development on its base. Computational Nanotechnology. 2015;**3**:11-25

[2] Flamant G, Ferriere A, Laplaze D, Monty C. Solar processing of materials: Opportunities and new frontiers. Solar Energy. 1999;**66**(2):117-132

[3] Trombe F, Gion L, Royere C, Robert JF. First results obtained with the 1000-kW solar furnace. Solar Energy. 1973;**15**:63-66

[4] Alvarez L, Guillard T, Olalde G, Rivoire B, Robert JF, Bernier P, et al. Large scale solar production of fullerenes and carbon nanotubes. Synthetic Metals. 1999;**103**(1–3):2476-2477

[5] Flamant G, Balat-Pichelin M. Elaboration and testing of materials using concentrated solar energy. In: Blanco Galvez J, Rodriguez SM, Delyannis E, Belessiotis VG, Bhattacharya SC, Kumar S, editors. Solar Energy Conversion and Photoenergy Systems. Vol. I. United Kingdom: Eolss Publishers Co., Ltd./UNESCO; 2010. pp. 363-389

[6] Riskiev TT, Abdurakhmanov AA, Khodjaev RA, Akbarov RY. The outlook for technical hydrogen production in the big solar furnace. Applied Solar Energy. 2003;**38**(4):49-54

[7] Fernandez-Gonzalez D et al. Concentrated solar energy applications in materials science and metallurgy. Solar Energy. 2018;**170**:520-540

[8] Herranz G, Rodriguez GP. Uses of concentrated solar energy in materials science. In: Rugescu RD, editor. Solar Energy. Croatia: InTech; 2010. pp. 146-170

[9] Azimov SA. Research-industrial complex Sun. Bimirror polyheliostat solar furnace with a thermal power of 1000 kW. Geliotekhnika. 1987;**6**:3-6 in Russian

[10] Abdurakhmanov AA, Akbarov RY, Gulamov KG, Riskiev TT. Operating experience of a big solar furnace 1000 kW in power. Applied Solar Energy. 1993;**34**(1):29-33

[11] Trombe F, Vinh ALP. Thousand kW solar furnace, built by the National Center of Scientific Research, in Odeillo (France). Solar Energy. 1973;**15**(1):57-61

[12] Riskiev TT, Suleimanov S.Kh. Double mirror polyheliostat solar furnace of 1000 kW thermal power. Solar Energy Materials. 1991;**24**(1–4):625-632

[13] Akbarov RY, Paizullakhanov MS. Characteristic features of the energy modes of a large solar furnace with a capacity of 1000 kW. Applied Solar Energy. 2018;**54**(2):99-109

[14] Abdurakhmanov AA, Akbarov RY, Sobirov YB, Yuldashev AA. Method of measurement and control of optical and geometric characteristics of mirrors and glasses. Applied Solar Energy. 2003;**39**(1):62-65

[15] Abdurakhmanov AA, Akbarov RY, Sobirov YB. Application of the system of technical vision in the big solar furnace. Applied Solar Energy. 1998;**34**(1):38-40

[16] Abdurakhmanov AA, Akbarov RY, Sobirov YB, Saribaev AS. A photometer for measuring the density of concentrated solar radiation. Applied Solar Energy. 2000;**36**(2):72-75

[17] Abdurakhmanov AA, Akbarov RY, Sobirov YB. Analysis of operating characteristics of various smelting

furnaces on a large solar furnace. Applied Solar Energy. 2008;**44**(1):24-27

[18] Abdurakhmanov AA, Akbarov RY, Sarybaev AS, Yuldashev AA. The automated control system of the heliostat field of the big solar furnace. Applied Solar Energy. 1998; **34**(1):34-37

[19] Atabaev IG, Akhatov ZS, Mukhamediev ED, Zievaddinov Z. Modernization of an automated controlling system for heliostat field of big solar furnace. Applied Solar Energy. 2016;**52**(3):220-225

[20] Faiziev SA, Sobirov YB. Measurements of solar resources in Uzbekistan. Applied Solar Energy. 2017; **53**(1):57-60

[21] Abdurakhmanov AA, Sobirov Yu B, Paizullakhonov MS, Orlov SA. Results of actinometric measurements at location of LSF with thermal capacity of 1000 kW. Applied Solar Energy. 2012; **48**(3):228-231

[22] Guillot E, Rodriguez R, Boullet N, Sans J-L. Some details about the third rejuvenation of the 1000 kWh solar furnace in Odeillo: Extreme performance heliostats. In: SolarPACES; 2017; Santiago, Chile: AIP Conference Proceedings; 2018. DOI: 10.1063/ 1.5067052

[23] Zakhidov RA, Weiner AA, Umarov G. Theory and Calculation of Applied Solar Energy Concentrating Systems (English Ed). Vadodara, India: Gujarat Energy Development Agency; 1992. p. 146

[24] Grilikhes VA, Matveev VM, Poluetkov VP. Solar high-temperature heat sources for spacecraft. Moscow: Mechanical Engineering; 1975. 248 p. (in Russian)

[25] Abdurakhmanov AA, Akbarov RY, Riskiev TT, Lewandowski A. On

calculation of optical-energetic characteristics of double mirror concentrating systems. Applied Solar Energy. 2002;**38**(2):71-77

[26] Klychev Sh I, Bakhramov SA, Zakhidov RA, Akbarov RY, Klycheva MS. Solar energy concentrators—Errors of numerical calculation of the irradiance integral for solar paraboloid concentrators. Applied Solar Energy. 2005;**41**(2):55-58

[27] Abdurakhmanov AA, Akbarov RY, Sarybaev AS, Yuldashev AA. A tower-type concentrator based on heliostats of a big solar furnace 1000 kW in power. Applied Solar Energy. 1999;**35**(2):60-65

[28] Akbarov RY, Pirmatov II, Riskiev TT. Specific features of the focal spot formation in big solar furnaces with polyheliostat systems. Applied Solar Energy. 1998;**34**(6):29-33

[29] Akbarov RY, Pirmatov II, Riskiev TT. Monitoring the energy density distribution in the focal zone of the big solar furnace. Applied Solar Energy. 1998;**34**(1):47-51

[30] Korn GA, Korn TM. Mathematical Handbook for Scientists and Engineers: Definitions, Theorems, and Formulas for Reference and Review. Mineola, New York: Dover publications, Inc.; 2000. 1151 pp

[31] Levin BR. Theoretical Basics of Statistical Radiotechnics, Book 1. Moscow: Soviet Radio Publ. Co.; 1969. 752 pp. (in Russian)